Progress In Electromagnetics Research B, Vol. 55, 277–295, 2013

A WALL-CLUTTER SUPPRESSION METHOD BASED ON SPATIAL SIGNATURE IN MIMO THROUGH-THE-WALL RADAR IMAGING

Lanzi Zhang*, Biying Lu, Zhimin Zhou, and Xin Sun

College of Electronic Science and Engineering, National University of Defense Technology, Changsha, Hunan 410073, China

Abstract—In through-the-wall radar imaging (TWRI), wall returns are often stronger than target returns, which make the targets behind walls invisible in the radar image. Spatial filtering that relies on the removal of the spatial zero-frequency components is a useful way for wall-clutter mitigation. Unfortunately, it applies to through-the-wall radar (TWR) with synthetic aperture array only. In this paper, a method based on spatial signature is proposed to suppress the wall-clutter in multi-input and multi-output (MIMO) TWRI. Firstly, the traditional spatial filtering method is discussed, as well as the reasons for the inapplicability for MIMO TWR. Secondly, the wall and target spatial signatures based on MIMO array are analyzed, respectively. The results indicate that the former has stability and symmetry, whereas the latter not. Thirdly, according to the above differences, a new method, symmetry subtraction, is applied to describe the wall-clutter suppression procedure. Finally, simulation results demonstrate that the proposed method is efficient in mitigating the wall returns and highlighting the targets.

1. INTRODUCTION

Through-the-Wall Radar Imaging (TWRI) can obtain two-dimensional high-resolution imagery of the objects through obstacles, which offers valuable information for target recognition or discrimination [1]. Therefore, TWRI becomes an emerging research field, driven by a growing need to several civilian and military sectors [2–5]. However, the existence of wall, which is often non-homogenous and/or non-uniform, results in heavy clutter that makes target image invisible.

Received 1 July 2013, Accepted 13 October 2013, Scheduled 16 October 2013

* Corresponding author: Lanzi Zhang (zhanglanzi5insist@aliyun.com).

Consequently, one of the important factors in TWRI for achieving a high-quality image is to use clutter suppression techniques so that the clutter as well as false target detection can be minimized.

In the past, there have been many studies conducted for suppressing clutter. Background subtraction [6, 7], which relies on the subtraction of the reference clutter (i.e., taking data in the absence of targets) from the measured data in the presence of the targets, is the most simple and effective method. However, in practice, it is not always feasible to have access to the background scene free from the targets of interest. Consequently, several approaches that estimate wall parameters are proposed [8–10]. Obviously, the target image is seriously affected by parameters estimation precision. In [11–14], statistical techniques, singular value decomposition (SVD), principal component analysis (PCA), factor analysis (FA), and independent component analysis (ICA), etc., have been applied in TWRI successfully. These techniques can enhance the target image without any priori information of wall or target. However, some clutter that has comparable energy to target signal may exist as ghosts [15, 16]. So, the further detection method must be taken into consideration.

In [17], spatial filtering is considered to be an effective way to suppress wall-clutter for through-the-wall radar (TWR). This method is implemented based on the assumption that the wall returns approximately are equal and have identical signal characteristics across the array elements in a monostatic mode, while target returns vary from sensor to sensor. Instead of relying on any priori knowledge of the wall parameters or background scene data, wall returns corresponding to spatial zero-frequency and low-frequency components can be separated from target returns by applying an appropriate spatial filter, such as notch filter. However, it should be noted that spatial filtering applies to TWR with synthetic aperture array only. Although synthetic aperture radar (SAR) techniques have been making steady progress in many fields, the long scanning time to achieve a high azimuth resolution as well as limitations of time and space make multi-input and multi-output (MIMO) radars more suitable [18–21]. Unfortunately, in bistatic mode, the wall returns received by different receivers are no longer identical. Therefore, the above-mentioned assumption must be dropped, namely, the traditional spatial filtering method is inapplicable. In this paper, we firstly pay emphasis on wall and target spatial signatures in MIMO TWRI. Theoretical analysis confirms that the former will be invariable when the antenna array position varies in cross-range direction, whereas the latter not. Significantly, for a specific array configuration, split transmit virtual aperture (STVA), the wall spatial signature is symmetric. In

view of the fact that the most MIMO arrays can be regarded as the combination of several STVA arrays, a new method, symmetry subtraction, is proposed to remove the symmetry part so as to mitigate undesired radar returns. Moreover, simulation results validate the effectiveness of the proposed method.

The paper is organized in the following way. Section 2 gives a brief introduction to traditional spatial filtering method as well as the reasons for the inapplicability for MIMO TWR. The wall and target spatial signatures based on MIMO array are presented in Section 3. After clarifying the differences between them, Section 4 proposes a new method, symmetry subtraction, to suppress wall-clutter. The effectiveness of the method is demonstrated in Section 5 followed by conclusion in Section 6.

2. SPATIAL SIGNATURE ANALYSIS IN SAR TWR

SAR concept is based on a single antenna, which transmits and receives the radar signal at one location, then moves to the next location and repeats the same operation along the axis parallel to the wall (see Fig. 1) [22, 23]. Assume that N antenna locations with spacing d. For simplicity, the wall is considered as an infinite slab.

For different antenna locations, the wall returns have the same time delay $\tau_W = 2R_W/c$ (where c is the speed of wave propagation), due to the perpendicular geometry between the main beam of the antenna and the wall. However, the time delays of target returns τ_{Tn}

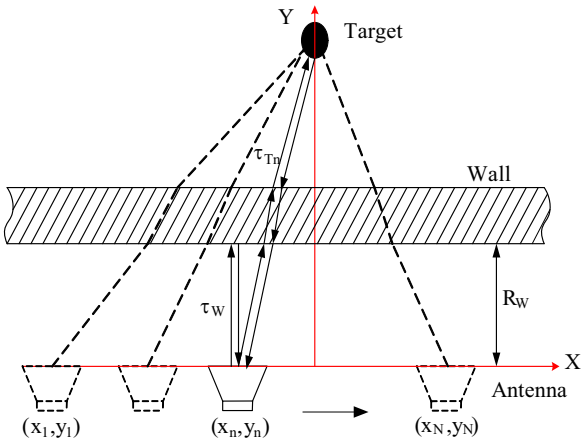

Figure 1. Imaging geometry of TWR with synthetic aperture array.

vary with different locations. The received echo of the nth location can be expressed as

$$\mathbf{S}_{\mathrm{Re}}(t,n) = \mathbf{S}_W(t-\tau_W) + \mathbf{S}_{Tg}(t-\tau_{Tn}) \tag{1}$$

where $\mathbf{S}_W$ and $\mathbf{S}_{Tg}$ are the returns from wall and target, respectively. Then, the echo matrix, or B-Scan matrix, is combined as follows

$$\mathbf{S} = [\mathbf{S}_{\mathrm{Re}}(t,1), \mathbf{S}_{\mathrm{Re}}(t,2), \ldots, \mathbf{S}_{\mathrm{Re}}(t,N)] \tag{2}$$

Suppose that the n_0th location is the closest to target with range R_{n_0}. The echo spatial signature after spatial frequency transform can be approximated as [17]

$$\mathbf{S}(\tau_{n_0},\kappa) \approx \mathbf{S}_W(\tau_{n_0}-\tau_W)\cdot\delta(\kappa) + \sum_{n=1}^{N} \mathbf{S}_{Tg}\left(-\frac{2r\,|n-n_0|\,d + (|n-n_0|d)^2}{R_{n_0}c}\right) \exp\left(-j2\pi\frac{\kappa}{N}n\right) \tag{3}$$

where $r = |x_p - x_{n_0}|$, x_p represents the cross-range location of the target, κ the spatial frequency, and $\delta(\cdot)$ the Dirac impulse function. According to (3), the zero-frequency component corresponds to constant returns, which is typical of wall, while target spatial signature has broad spectral range. Therefore, a proper filter, such as notch filter, can be applied to separate the above-mentioned two signals. Meanwhile, it should be noted that the method loses a part of target information due to the overlapping between wall and target spatial signature.

However, this approach is inapplicable to MIMO radar, because the time delay τ_W in (1) changes with antenna locations. So, wall spatial signature also has wide spatial frequency band after transform. Consequently, the wall and target spatial signature in MIMO TWRI will come under review in next section.

3. SPATIAL SIGNATURE ANALYSIS IN MIMO TWR

In recently years, MIMO radars have attracted great interest. A MIMO array with M transmitters and N receivers can obtain a virtual aperture with $M \times N$ virtual transceivers, which yields lighter-weight, lower-cost systems and higher imaging quality as compared with SAR array of comparable performance. Therefore, the MIMO techniques are more suitable to TWR. On the basis of our previous work, a specific array configuration, STVA, has been successfully applied to TWR and forward-looking ground penetrating radar (FLGPR), because of its well imaging and detection performance [24]. In addition, most MIMO arrays can be viewed as the combination of several STVA arrays.

Thus, the returns from TWR with this typical array structure will be analyzed in the following content.

3.1. Wall and Point Target Spatial Signatures

The MIMO radar system transmits stepped-frequency signal with M frequency point to detect the targets behind walls, which can be expressed as

$$S_{Tr}(t) = \sum_{m=0}^{M-1} \text{rect}\left(\frac{t - mT_p - T_p/2}{T_p}\right) \exp\left(j2\pi f_m t\right) \tag{4}$$

where the variable T_p is the pulse duration and f_m the mth frequency. Generally speaking, walls are considered as homogeneous dielectric slabs, so its electromagnetic characteristics can be described by concise mathematical models. The permittivity and thickness of the wall are ε_r and D, respectively. The MIMO array in this paper is composed of two transmitters and a linear receiving array of N receivers equally spaced located along the X-axis. The two transmit elements are located at the two ends of the receiving array and work sequentially. To simplify the derivation, assume that array and target are at the same height. Fig. 2 shows the propagation procedure of the electromagnetic wave.

Consider transmitter/receiver (T/R) pair $\{T_q, R_n\}$, i.e., the waveform is transmitted by qth transmitter and received by the nth receiver located at $\mathbf{r}_{T_q} = (x_{T_q}, y_{T_q})$ and $\mathbf{r}_{R_n} = (x_{R_n}, y_{R_n})$, respectively. The point target location is $\mathbf{r}_P = (x_p, y_p)$. Therefore, the received

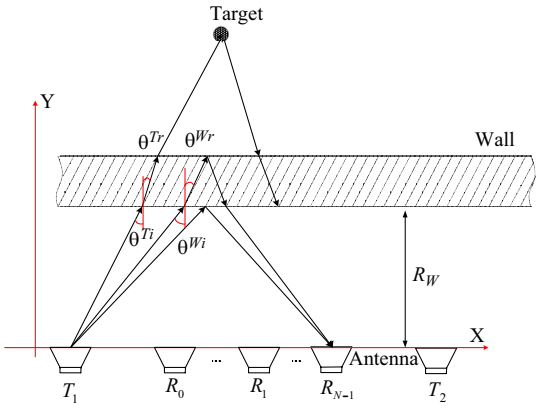

Figure 2. The propagation procedure of electromagnetic wave in MIMO TWRI.

signal with the T/R pair is

$$\mathbf{S}_{\mathrm{Re}}(\varpi_m, \mathbf{r}_{T_q}, \mathbf{r}_{R_n}) = \mathbf{S}_W(\varpi_m, \mathbf{r}_{T_q}, \mathbf{r}_{R_n}) + \mathbf{S}_{Tg}(\varpi_m, \mathbf{r}_{T_q}, \mathbf{r}_{R_n}, \mathbf{r}_P) \quad (5)$$

where $\varpi_m = 2\pi f_m/c$ is the wavenumber, $\mathbf{S}_W(\varpi_m, \mathbf{r}_{T_q}, \mathbf{r}_{R_n})$ and $\mathbf{S}_{Tg}(\varpi_m, \mathbf{r}_{T_q}, \mathbf{r}_{R_n}, \mathbf{r}_P)$ are the wall and target returns, respectively. Then, the two signals will be discussed separately.

As shown in Fig. 2, a part of transmit signal is directly reflected by the front side of the wall, and the rest has experienced multiple reflections inside the wall. Therefore, the wall reflection is approximately expressed as [25, 26]

$$\mathbf{S}_W(\varpi_m, \mathbf{r}_{T_q}, \mathbf{r}_{R_n}) \approx \frac{\sigma^W}{R_{qn}^W} \exp\left[-j\varpi_m \tau_{qn}^W c\right] \cdot \mathbf{\Psi}^*(\varpi_m, \mathbf{r}_{T_q}, \mathbf{r}_{R_n}) \quad (6)$$

where the superscript * is the complex conjugate operator and σ^W is the amplitude factor. From simple geometric considerations, the travel length is $R_{qn}^W = \sqrt{(x_{T_q} - x_{R_n})^2/4 + R_W^2}$, and time delay satisfies $\tau_{qn}^W = 2R_{qn}^W/c$. Assume that $\varpi_m^F = \varpi_m \cos\theta_{qn}^{Wi}$ and $\varpi_m^W = \varpi_m \cos\theta_{qn}^{Wr}$ are the normal propagation wavenumber in the air and the dielectric, respectively, where θ_{qn}^{Wi} is incidence angle, and θ_{qn}^{Wr} is refraction angle. Thus, the reflection coefficient of the wall is given by [27]

$$\mathbf{\Psi}(\varpi_m, \mathbf{r}_{T_q}, \mathbf{r}_{R_n}) = \frac{-\dfrac{1-\eta}{1+\eta} + \dfrac{1-\eta}{1+\eta}\exp\left(j2\varpi_m^W D\right)}{1 - \left(\dfrac{1-\eta}{1+\eta}\right)^2 \exp\left(j2\varpi_m^W D\right)} \quad (7)$$

where variable η may be $\eta^h = \varepsilon_r \varpi_m^F/\varpi_m^W$ or $\eta^v = \varpi_m^F/\varpi_m^W$, and the superscript h or v denotes vertically or horizontally polarized incident waves. Space constraints permit only the former to be discussed. Substitute (7) into (6), $\mathbf{S}_W$ can be expressed as follows:

$$\mathbf{S}_W(\varpi_m, \mathbf{r}_{T_q}, \mathbf{r}_{R_n}) \approx \sigma_{qn}^W \frac{-\dfrac{\cos\theta_{qn}^{Wr} - \varepsilon_r \cos\theta_{qn}^{Wi}}{\cos\theta_{qn}^{Wr} + \varepsilon_r \cos\theta_{qn}^{Wi}} + \dfrac{\cos\theta_{qn}^{Wr} - \varepsilon_r \cos\theta_{qn}^{Wi}}{\cos\theta_{qn}^{Wr} + \varepsilon_r \cos\theta_{qn}^{Wi}} \exp\left(-j2\varpi_m \cos\theta_{qn}^{Wr} D\right)}{1 - \left(\dfrac{\cos\theta_{qn}^{Wr} - \varepsilon_r \cos\theta_{qn}^{Wi}}{\cos\theta_{qn}^{Wr} + \varepsilon_r \cos\theta_{qn}^{Wi}}\right)^2 \exp\left(-j2\varpi_m \cos\theta_{qn}^{Wr} D\right)} \exp\left(-\frac{j2\varpi_m R_W}{\cos\theta_{qn}^{Wi}}\right) \quad (8)$$

where $\cos\theta_{qn}^{Wi} = R_W \Big/ \sqrt{(x_{T_q} - x_{R_n})^2/4 + R_W^2}$, and the refraction angle is figured out with Snell law. From (8), we can know that wall returns are decided by the distance between transmitter and receiver.

As for target returns, the propagation procedure of the incident wave is transmitted by T_q to the target and the target's scattered wave received by R_n. At the same time, the target returns have passed through the wall twice in the process. Thus, the demodulated target echo is approximately given by [25, 26]

$$\begin{aligned}&\mathbf{S}_{Tg}(\varpi_m, \mathbf{r}_{T_q}, \mathbf{r}_{R_n}, \mathbf{r}_P)\\ \approx\ &\frac{\sigma^T}{R_{qp}^T R_{pn}^T}\exp\left[-j\varpi_m\tau_{qn}^T c\right]\cdot\mathbf{\Phi}_1^*(\varpi_m, \mathbf{r}_{T_q}, \mathbf{r}_p)\mathbf{\Phi}_2^*(\varpi_m, \mathbf{r}_p, \mathbf{r}_{R_n})\end{aligned} \quad (9)$$

where σ^T is the amplitude factor, time delay is $\tau_{qn}^T = \left[R_{qp}^T + R_{pn}^T\right]/c$, for $R_{qp}^T = \left|\mathbf{r}_p - \mathbf{r}_{T_q}\right|$ and $R_{pn}^T = |\mathbf{r}_{R_n} - \mathbf{r}_p|$. $\mathbf{\Phi}_1(\varpi_m, \mathbf{r}_{T_q}, \mathbf{r}_p)$ and $\mathbf{\Phi}_2(\varpi_m, \mathbf{r}_p, \mathbf{r}_{R_n})$ are the transmission coefficients. Likewise, for horizontally polarized incident waves, $\mathbf{\Phi}_1$ is defined as [27]

$$\begin{aligned}&\mathbf{\Phi}_1(\varpi_m, \mathbf{r}_{T_q}, \mathbf{r}_p)\\ =\ &\frac{4\cdot\exp\left[j\varpi_m\left(\sqrt{\varepsilon_r}\cos\theta_{qn}^{Tr} - \cos\theta_{qn}^{Ti}\right)D\right]}{\left(1+\dfrac{\sqrt{\varepsilon_r}\cos\theta_{qn}^{Ti}}{\cos\theta_{qn}^{Tr}}\right)\left(1+\dfrac{\cos\theta_{qn}^{Tr}}{\sqrt{\varepsilon_r}\cos\theta_{qn}^{Ti}}\right)}\\ &\left\{1-\left(\frac{\cos\theta_{qn}^{Tr}-\sqrt{\varepsilon_r}\cos\theta_{qn}^{Ti}}{\cos\theta_{qn}^{Tr}+\sqrt{\varepsilon_r}\cos\theta_{qn}^{Ti}}\right)^2\exp\left(j2\varpi_m\sqrt{\varepsilon_r}\cos\theta_{qn}^{Tr}D\right)\right\}\end{aligned} \quad (10)$$

With [28],

$$\cos\theta_{qn}^{Ti} = R_W\Bigg/\sqrt{\left\{\frac{\begin{array}{c}|x_p - x_{n_0}|\cdot R_W[\sqrt{\varepsilon_r}(|y_p\\ -D-R_W|+D)-D]\end{array}}{\begin{array}{c}\sqrt{\varepsilon_r}(R_W+|y_p-D-R_W|)\\ (|y_p-D-R_W|+D)-DR_W\end{array}}\right\}^2 + R_W^2} \quad (11)$$

Obviously, unlike wall returns, target returns are related to not only the distance between transmitter and receiver, but also target position.

The signal after pulse compression is

$$\mathbf{S}_{RT}(k, \mathbf{r}_T, \mathbf{r}_R) = \mathcal{IFFT}_{\varpi_m\to k}\left\{\mathbf{S}_{\mathrm{Re}}(\varpi_m, \mathbf{r}_{T_q}, \mathbf{r}_{R_n})\right\} \quad (12)$$

where $\mathcal{IFFT}_{\varpi_m\to k}[\cdot]$ is the inverse Fourier transform with respect to ϖ_m. Take $\mathbf{S}_{RT}(k, id)$ instead of $\mathbf{S}_{RT}(k, \mathbf{r}_{T_q}, \mathbf{r}_{R_n})$, where $id = n + (q-1)N$, for $q = 1, 2$ and $n = 0, \ldots, N-1$. The B-Scan matrix can be expressed as

$$\mathbf{S} = [\mathbf{S}_{RT}(k, 1), \mathbf{S}_{RT}(k, 2), \ldots, \mathbf{S}_{RT}(k, 2N)] \quad (13)$$

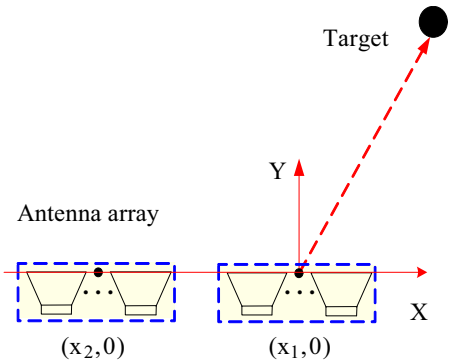

Figure 3. Illustration of the antenna array position.

Converting the result to spatial domain as

$$\mathbf{S}_{Spa} = \mathcal{FFT}_{id\to\kappa}\{\mathbf{S}\} \tag{14}$$

where $\mathcal{FFT}_{id\to\kappa}[\cdot]$ is the Fourier transform with respect to id. $\mathbf{S}_{Spa}$ represents echo spatial signature of MIMO radar. Suppose that the array center is placed at two different positions $(x_1, 0)$ and $(x_2, 0)$, respectively (see Fig. 3), $\mathbf{S}_{Spa}$ can be expressed as follows:

$$\begin{aligned} \mathbf{S}_{Spa}^{(x_1)} &= \mathbf{S}_{WSpa}^{(x_1)} + \mathbf{S}_{TSpa}^{(x_1)} \\ \mathbf{S}_{Spa}^{(x_2)} &= \mathbf{S}_{WSpa}^{(x_2)} + \mathbf{S}_{TSpa}^{(x_2)} \end{aligned} \tag{15}$$

where $\mathbf{S}_{WSpa}$ and $\mathbf{S}_{TSpa}$ are wall and target spatial signature, respectively. Based on the above results, we can know that $\mathbf{S}_{WSpa}^{(x_1)} = \mathbf{S}_{WSpa}^{(x_2)}$, and $\mathbf{S}_{TSpa}^{(x_1)} \neq \mathbf{S}_{TSpa}^{(x_2)}$.

Obviously, wall spatial signature remains unchanged with different array positions in cross-range direction, whereas target spatial signature changes a lot. The differences make it possible for us to separate wall and target returns based on their spatial signatures.

3.2. Canonical Area Target Spatial Signature

In practical applications, the target is not ideal point target used above, such as human body or furniture. Consequently, spatial signatures of different type of targets are necessary to be analyzed. In order to obtain the scattering feature of different scatterers, the measurements need be

carried out with no electromagnetic interference. However, the major disadvantage lies in its different parameters such as size or location, which leads to a large computational burden. Therefore, parametric models of scatterers play an important role. According to the geometric theory of diffraction (GTD), the high-frequency scattering response from a complex object can be well modeled by the sum of responses from individual scatterers [29]. GTD-based parametric models not only provide a physically relevant representation of the scattering behavior but also conform to actual condition. In [30], bistatic scattering models for canonical scatterers, rectangular plate, dihedral, trihedral, cylinder, top-hat, etc., have been proposed, which offer benefits to area target spatial signature analysis.

Use the same array configuration in Section 3.1, the transmitter position $\mathbf{r}_T$ and the transmitter position $\mathbf{r}_R$ can be expressed as follows:

$$\begin{aligned}\mathbf{r}_T &= (x_T, y_T, z_T) = R_T(\cos\gamma_T\cos\varphi_T, \cos\gamma_T\sin\varphi_T, \sin\gamma_T)\\ \mathbf{r}_R &= (x_R, y_R, z_R) = R_R(\cos\gamma_R\cos\varphi_R, \cos\gamma_R\sin\varphi_R, \sin\gamma_R)\end{aligned} \tag{16}$$

where $R_T = \sqrt{(x_p - x_T)^2 + (y_p - y_T)^2 + (z_p - z_T)^2}$ and $R_R = \sqrt{(x_p - x_R)^2 + (y_p - y_R)^2 + (z_p - z_R)^2}$. Angle pairs (γ_T, φ_T) and (γ_R, φ_R) describe the transmitter and receiver locations in elevation and azimuth. Thus, we represent the echo as

$$\begin{aligned}&\mathbf{S}_{\mathrm{Re}}(\varpi_m, \mathbf{r}_T, \mathbf{r}_R, \Theta_\Omega)\\ &= \sum_{\Omega} \mathbf{P}_\Omega \mathbf{M}_{\Gamma(\Omega)}(\varpi_m, \mathbf{r}_T, \mathbf{r}_R, \Theta_\Omega) \exp\left[j\varpi_m \Delta R_{\Gamma(\Omega)}(\mathbf{r}_T, \mathbf{r}_R, \Theta_\Omega)\right]\end{aligned} \tag{17}$$

where Θ_Ω describes physical parameters of scatterers, including location, orientation and size. $\mathbf{P}_\Omega$ captures the scatterers' polarization dependence. $\mathbf{M}_{\Gamma(\Omega)}(\varpi_m, \mathbf{r}_T, \mathbf{r}_R, \Theta_\Omega)$ contains function shape response of the Ωth scatterer, and the subscripts $\Gamma(\Omega)$ denotes type of canonical scatterer. $\Delta R_{\Gamma(\Omega)}(\mathbf{r}_T, \mathbf{r}_R, \Theta_\Omega)$ presents propagation length.

Take three typical scatterers in TWRI for example, namely, dihedral, trihedral and cylinder (as shown in Fig. 4). Their scattering responses are in turn modeled as [30]

$$\begin{aligned}&M_{di}(\varpi_m, \mathbf{r}_T, \mathbf{r}_R, \Theta_\Omega)\\ &= \frac{j2\varpi_m LH}{\sqrt{\pi}} \mathrm{sinc}\left[\varpi_m \frac{L}{2}(\sin\varphi_T\cos\gamma_T + \sin\varphi_R\cos\gamma_R)\right]\\ &\quad \times \mathrm{sinc}\left[\varpi_m H(\cos\gamma_T - \cos\gamma_R)\right] \cdot \begin{cases} \sin\left(\dfrac{\gamma_T+\gamma_R}{2}\right), \gamma_T, \gamma_R \in \left[0, \dfrac{\pi}{4}\right] \\ \cos\left(\dfrac{\gamma_T+\gamma_R}{2}\right), \gamma_T, \gamma_R \in \left[\dfrac{\pi}{4}, \dfrac{\pi}{2}\right] \end{cases}\end{aligned} \tag{18}$$

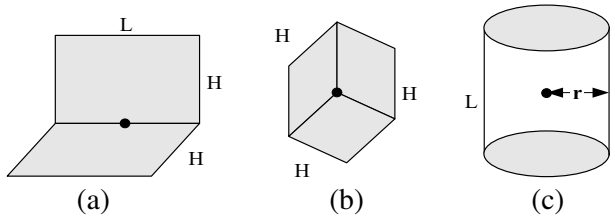

Figure 4. The size parameters. (a) Dihedral, (b) trihedral, (c) cylinder.

$$
\begin{aligned}
&M_{tr}(\varpi_m, \mathbf{r}_T, \mathbf{r}_R, \Theta_\Omega) = \frac{j\varpi_m\sqrt{3}H^2}{\sqrt{\pi}}\mathrm{sinc}\left[\varpi_m H(\cos\gamma_T - \cos\gamma_R)\right] \\
&\left\{\mathrm{sinc}\left\{\varpi_m H\left[\cos\left(\varphi_R - \frac{\pi}{4}\right)\cos\gamma_R - \cos\left(\varphi_T - \frac{\pi}{4}\right)\cos\gamma_T\right]\right\}\right. \\
&\left.+ \mathrm{sinc}\left\{\varpi_m H\left[\cos\left(\varphi_R + \frac{\pi}{4}\right)\cos\gamma_R - \cos\left(\varphi_T + \frac{\pi}{4}\right)\cos\gamma_T\right]\right\}\right\} \\
&\cdot\begin{Bmatrix} \sin\left(\frac{\gamma_T+\gamma_R}{2} + \frac{\pi}{4} - \tan^{-1}\left(\frac{1}{\sqrt{2}}\right)\right), \gamma_R \in \left[0, \tan^{-1}\left(\frac{1}{\sqrt{2}}\right)\right] \\ \cos\left(\frac{\gamma_T+\gamma_R}{2} + \frac{\pi}{4} - \tan^{-1}\left(\frac{1}{\sqrt{2}}\right)\right), \gamma_R \in \left[\tan^{-1}\left(\frac{1}{\sqrt{2}}\right), \frac{\pi}{2}\right] \end{Bmatrix} \\
&\cdot\begin{Bmatrix} -\cos\left(\frac{\varphi_T+\varphi_R}{2} - \frac{\pi}{4}\right), \varphi_R \in \left[-\frac{\pi}{4}, 0\right] \\ \sin\left(\frac{\varphi_T+\varphi_R}{2} - \frac{\pi}{4}\right), \varphi_R \in \left[0, \frac{\pi}{4}\right] \end{Bmatrix} \qquad (19)
\end{aligned}
$$

$$
\begin{aligned}
&M_{cy}(\varpi_m, \mathbf{r}_T, \mathbf{r}_R, \Theta_\Omega) \\
&= \sqrt{\frac{j\varpi_m r}{\cos\varphi_T}} H\cos\varphi_R \times \mathrm{sinc}\left[\frac{\varpi_m H}{2}(\sin\varphi_T\cos\gamma_T + \sin\varphi_R\cos\gamma_R)\right] \qquad (20)
\end{aligned}
$$

where φ_T, φ_R, γ_T, $\gamma_R \in [-\pi/2, \pi/2]$. After calculating the echo, their spatial signatures can be obtained easily with the same approach in Section 3.1.

It is clear that φ_T, φ_R, γ_T and γ_R are important parameters in building the echo. In other words, the spatial signatures of above scatterers are closely connected with array and scatterer locations, like point target. Therefore, it provides theoretical foundation to suppress wall-clutter according to the differences between wall and target spatial signature.

4. WALL-CLUTTER SUPPRESSION METHOD

Although we know that the wall spatial signature is invariable in cross-range direction, it is insufficient to provide the required information to

separate wall and target returns. Then, a more detailed analysis is conducted in this section.

Considering the configuration of MIMO array, the wall reflections received by T/R pairs $\{T_1, R_n\}$ and $\{T_2, R_{N-n-1}\}$ have the relationship as

$$\mathbf{S}_W(\varpi_m, \mathbf{r}_{T_1}, \mathbf{r}_{R_n}) = \mathbf{S}_W(\varpi_m, \mathbf{r}_{T_2}, \mathbf{r}_{R_{N-n-1}}) \tag{21}$$

According to the properties of spatial frequency transform, we modify the echo a little bit, adding a column of zero elements to the end of raw matrix, which will benefit the further analysis without affecting the returns. After the transform, wall spatial signature is given as

$$\mathbf{S}_{WSpa}(k, \kappa) = \mathbf{S}_{WSpa}(k, 2N - \kappa + 2), \quad \kappa = 1, \ldots, 2N + 1 \tag{22}$$

Thus, matrix $\mathbf{S}_{Spa}$ can be written as

$$\mathbf{S}_{Spa}(k, \kappa) = \left[\mathbf{S}^{(1)}_{Spa}(k, \kappa), \mathbf{S}_{Spa}(k, N + 1), \mathbf{S}^{(2)}_{Spa}(k, \kappa)\right] \tag{23}$$

what's more,

$$\begin{aligned} \mathbf{S}^{(1)}_{Spa}(k, \kappa) &= \mathbf{S}^{(1)}_{WSpa}(k, \kappa) + \mathbf{S}^{(1)}_{TSpa}(k, \kappa), \quad \kappa = 1, \ldots, N \\ \mathbf{S}^{(2)}_{Spa}(k, \kappa) &= \mathbf{S}^{(2)}_{WSpa}(k, \kappa) + \mathbf{S}^{(2)}_{TSpa}(k, \kappa), \quad \kappa = N + 2, \ldots, 2N + 1 \end{aligned} \tag{24}$$

Plugging (22) into (24), $\mathbf{S}^{(2)}_{Spa}(k, \kappa)$ can be expressed as

$$\begin{aligned} \mathbf{S}^{(2)}_{Spa}(k, \kappa) = \mathbf{S}^{(1)}_{WSpa}(k, 2N - \kappa + 2) + \mathbf{S}^{(2)}_{TSpa}(k, \kappa), \\ \kappa = N + 2, \ldots, 2N + 1 \end{aligned} \tag{25}$$

Equation (25) indicates that the wall spatial signature is symmetric. Therefore, as a new method, symmetry subtraction that aims at subtracting the symmetry part (i.e., wall-clutter) from raw echo spatial signature is proposed.

Due to the weak target signal, we can take the less value between $\mathbf{S}^{(1)}_{Spa}(k, \kappa)$ and $\mathbf{S}^{(2)}_{Spa}(k, \kappa)$ as the estimation of wall spatial signature, which is defined as

$$\hat{\mathbf{S}}_{WSpa}(k, \kappa) = \min\left\{\mathbf{S}_{Spa}(k, \kappa), \mathbf{S}_{Spa}(k, 2N - \kappa + 2)\right\} \tag{26}$$

Eliminating the undesirable spatial signature, the new echo spatial signature is

$$\mathbf{S}'_{Spa}(k, \kappa) = \mathbf{S}_{Spa}(k, \kappa) - \hat{\mathbf{S}}_{WSpa}(k, \kappa) \tag{27}$$

After the transformation from the time domain to spatial domain and discarding the last column (i.e., the additional column), we can obtain the new echo after wall-clutter suppression.

It is important to note that most MIMO arrays consist of several STVA arrays. Consequently, the data collected by each STVA array can be processed with the proposed method in this paper, and then recombine them to produce the new B-Scan matrix. The flow diagram of the algorithm is described in Fig. 5.

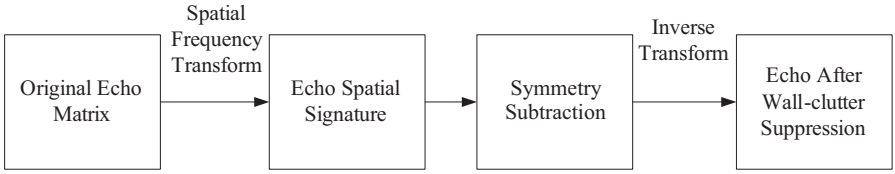

Figure 5. Calculating the echo matrix after wall-clutter suppression.

5. SIMULATIONS

In order to verify the effectiveness of the proposed method, an exact field computation method, finite-difference time-domain (FDTD), is employed to model the electromagnetic (EM) scattering problem [31, 32]. The original excitation pulse in the FDTD simulations is a Gaussian pulse, covering the bandwidth from 0.5 to 2.0 GHz. The FDTD grid has a resolution (cubic cell size) of 10 mm, which is decided by the frequency of excitation (Hz). The antenna array is parallel to the wall, and the distance between them is 1.7 m. The array has 2 transmitters and 21 receivers with 0.05 m interval.

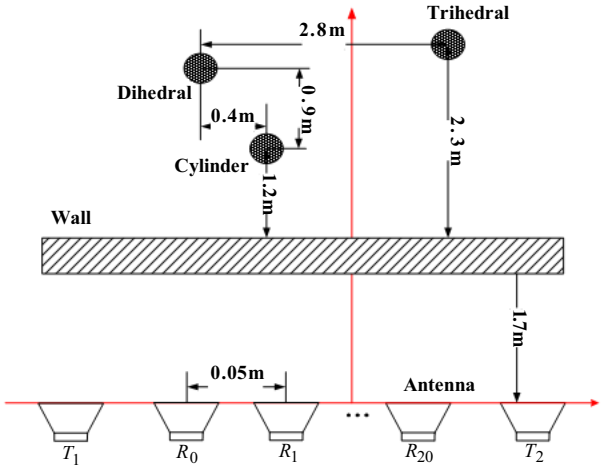

Figure 6. FDTD simulation scene layout.

5.1. Three Scatters behind the Wall

The first scenario we analyze is the imaging of a simple front wall with a dihedral, a trihedral and a cylinder placed behind the wall, as shown in Fig. 6. The dimensions of scenario that is considered for simulations are $4\,\mathrm{m} \times 5\,\mathrm{m} \times 2.2\,\mathrm{m}$. The brick walls are made of a uniform dielectric with permittivity $\varepsilon_r = 3.8$ and conductivity $\sigma = 0.02\,\mathrm{S/m}$ [33].

The BP imaging results with different methods are shown in Fig. 7. The upper-left image corresponds to the unprocessed case, which indicates that strong reflections from the walls obscures the target information. From Figs. 7(b) and (c), it is perceptible that

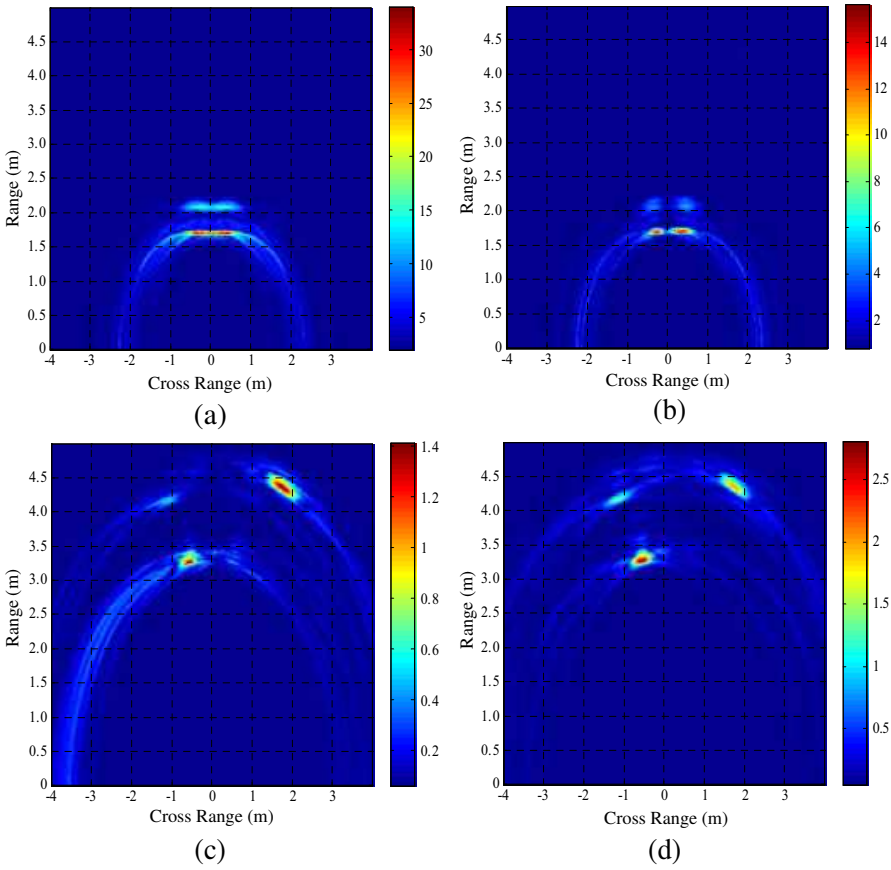

Figure 7. Radar images. (a) With wall returns, (b) with spatial filtering, (c) with symmetry subtraction, (d) with background subtraction.

spatial filtering does not apply to MIMO TWR, whereas symmetry subtraction method can suppress the wall-clutter efficiently and the "targets" behind the wall are highlighted. To prove that the "targets" are true targets, the image with background subtraction is shown in Fig. 7(d). It is clear that symmetry subtraction method is efficient in reducing wall-clutter in MIMO TWRI.

For a more detailed explanation, the spatial signatures corresponding to the above cases are shown in Fig. 8. Obviously, wall spatial signature yields symmetry (Fig. 8(a)), and target returns will be covered even though we remove the zero-frequency part (Fig. 8(b)). Figs. 8(c) and (d) illustrate that the wall returns can be eliminated by mitigating the symmetry component in echo spatial signature, which is consistent with our previous theoretical analysis.

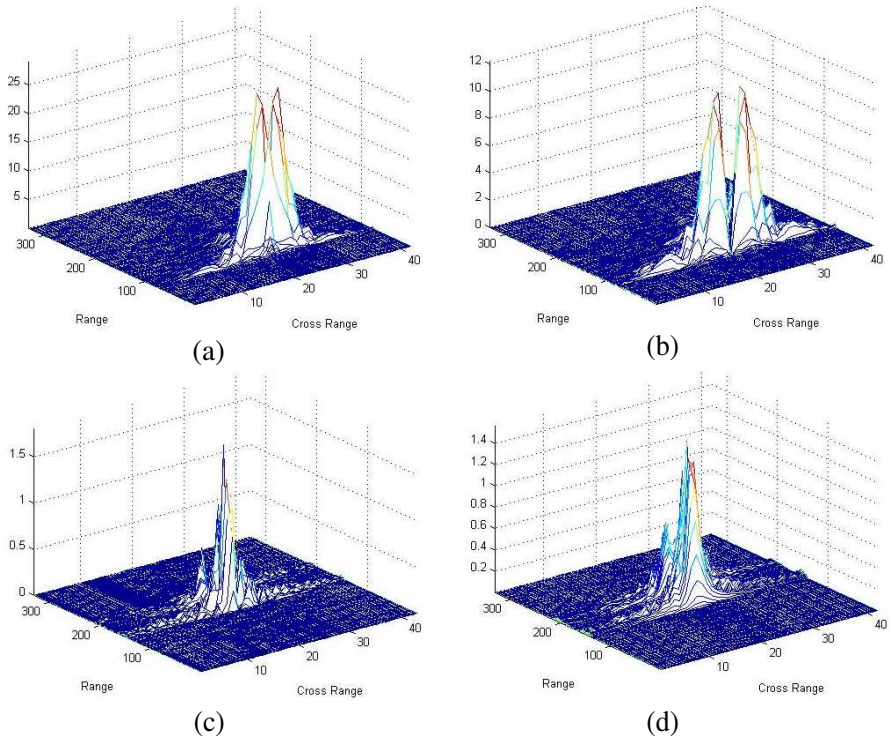

Figure 8. Spatial signatures. (a) With wall returns, (b) with spatial filtering, (c) with symmetry subtraction, (d) with background subtraction.

5.2. Human in a Brick Room

In the following experiments, a more complicated scenario, as shown in Fig. 9, is considered, where two humans are placed in a four-wall concrete building ($\varepsilon_r = 6.8$, $\sigma = 0.1\,\mathrm{S/m}$) with a small brick room. The complex building overall dimensions are $5\,\mathrm{m} \times 3.7\,\mathrm{m} \times 2.8\,\mathrm{m}$, two humans with the height of 1.75 m are 1 m and 1.3 m away from the front wall, respectively, and the distance between them in cross-range direction is 2.6 m.

The imaging results with wall returns, symmetry subtraction and background subtraction are clearly indicated by the dashed line in Figs. 10–12. Clearly, the targets with weak reflections are illuminated

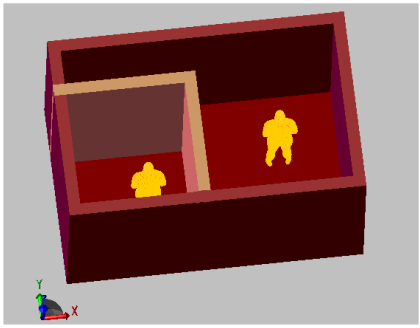

Figure 9. FDTD simulation scenario.

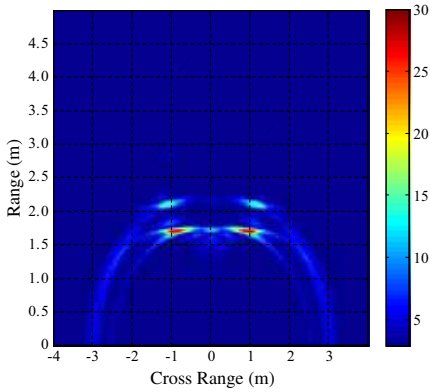

Figure 10. The image with wall returns.

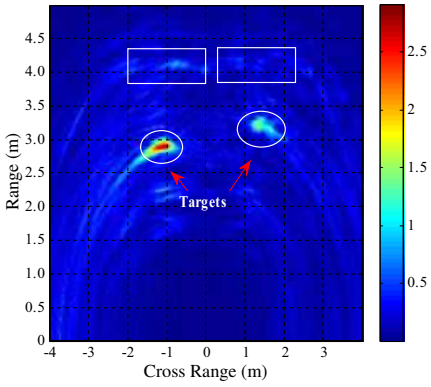

Figure 11. The image with symmetry subtraction.

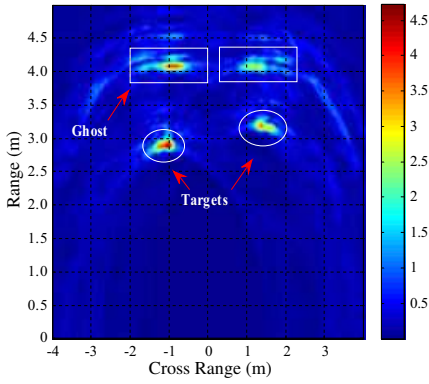

Figure 12. The image with background subtraction.

with strong responses after wall-clutter suppression. It is noteworthy that, compared to Fig. 11, we find some ghosts (in white boxes) in Fig. 12. This is because some back wall returns in reference clutter are left after using background subtraction. The targets positions (in white circles) in Fig. 11 prove not only the good accordance with the real scene but also the effectiveness of our proposed method.

6. CONCLUSIONS

Considering that wall-clutter has a bad effect on the imaging of target in TWRI, an attempt has been made to develop a clutter reduction technique for MIMO TWRI. Through the theoretical analysis of echo spatial signature, it is found that unlike target, wall spatial signature will not vary with antenna array positions in cross-range direction. Moreover, wall spatial signature is symmetric, when TWR operates with a STVA array. Thanks to the fact that most MIMO arrays can be viewed as the combination of several STVA arrays, symmetry subtraction that aims at removing the symmetry part (i.e., wall-clutter) is proposed. The results in Section 5 prove that the method works well in suppressing wall-clutter. Furthermore, based on the preliminary analysis in this paper, we are able to infer much vital information about different types of targets from their spatial signatures, which constitute subjects of current and future investigations.

ACKNOWLEDGMENT

This work was supported by the National Natural Science Foundation of China under Grants 61372161 and 61271441, the Foundation for the Author of National Excellent Doctoral Dissertation of China under Grant 201046.

REFERENCES

1. Amin, M. G., *Through-the-Wall Radar Imaging*, CRC Press, Boca Raton, FL, 2011.
2. Sisma, O., A. Gaugue, C. Liebe, and J. M. Ogier, "UWB radar: Vision through a wall," *Personal Wireless Communications*, Vol. 245, 241–251, 2007.
3. Baranoski, E. J., "Through wall imaging: Historical perspective and future directions," *IEEE International Conference on*

Acoustics, Speech and Signal Processing, ICASSP, 5173–5176, 2008.

4. Borek, S. E., "An overview of through the wall surveillance for homeland security," *Proceedings of the 34th Applied Imagery and Pattern Recognition Workshop (AIPR05)*, 6, 2005.
5. Lubecke, V. M. and A. E. Fathy, "Through-the-wall radar life detection and monitoring," *IEEE Microwave Symposium*, 769–772, 2007.
6. Piccardi, M., "Background substraction techniques: A review," *IEEE International Conference on Systems, Man and Cybernetics*, Vol. 4, 3099–3104, 2004.
7. Ahmad, F. and M. G. Amin, "Through-the-wall radar imaging experiments," *IEEE Workshop on Signal Processing Applications for Public Security and Forensics, SAFE-07*, 1–5, 2007.
8. Wang, G. and M. G. Amin, "Imaging through unknown walls using different standoff distances," *IEEE Trans. on Signal Processing*, Vol. 54, No. 10, 4015–4025, 2006.
9. Jin, T., B. Chen, and Z. Zhou, "Image-domain estimation of wall parameters for autofocusing of through-the-wall SAR imagery," *IEEE Trans. on Geosci. Remote Sens.*, Vol. 51, No. 3, 1836–1843, 2013.
10. Ahmad, F., M. G. Amin, and S. A. Kassam, "Synthetic aperture beamformer for imaging through a dielectric wall," *IEEE Trans. on Aerosp. Electron.*, Vol. 41, No. 1, 271–283, 2005.
11. Verma, P. K., A. N. Gaikwad, D. Singh, and M. J. Nigam, "Analysis of clutter reduction techniques for through wall imaging in UWB radar," *Progress In Electromagnetics Research B*, Vol. 17, 29–48, 2009.
12. Gaikwad, A. N., D. Singh, and M. J. Nigam. "Application of clutter reduction techniques for detection of metallic and low dielectric target behind the brick wall by stepped frequency continuous wave radar in ultra-wideband range," *IET Radar Sonar and Navigation*, Vol. 5, No. 4, 416–425, 2011.
13. Ahmad, F. and M. G. Amin, "Wall clutter mitigation for MIMO radar configurations in urban sensing," *Signal Processing for Communication, Radar and Sonar*, 1165–1170, 2012.
14. Tivive, F. H. C., A. Bouzerdoum, and M. G. Amin, "An SVD-based approach for mitigating wall reflections in through-the-wall radar imaging," *Proceedings of IEEE Radar Conference*, 519–524, 2011.

15. Zhang, L., B. Lu, Z. Zhou, and X. Sun, "The clutter suppression based on FA and image contrast in TWI application," *Proceedings of 2013 Third IEEE International Conference on Information Science and Technology (ICIST 2013)*, 1498–1502, 2013.
16. Zhang, L., B. Lu, Z. Zhou, and X. Sun, "The clutter suppression based on statistical techniques in TWI application," *Proceedings of 2013 IEEE International Conference on Ultra-wideband (ICUWB 2013)*, 130–135, 2013.
17. Yoon, Y. S. and M. G. Amin, "Spatial filtering for wall-clutter mitigation in through-the-wall radar imaging," *IEEE Trans. on Geosci. Remote Sens.*, Vol. 47, No. 9, 3192–3208, 2009.
18. Haimovich, A. M., R. S. Blum, and L. J. Cimini, "MIMO radar with widely separated antennas," *IEEE Signal Processing Magazine*, Vol. 25, No. 1, 116–129, 2008.
19. Schwartz, J. L. and B. D. Steinberg, "Ultrasparse, ultrawideband arrays," *IEEE Transactions on Ultrasonics, Ferroelectrics, and Frequency Control*, Vol. 45, No. 2, 376–393, 1998.
20. Jin, T., J. Lou, and Z. Zhou, "Extraction of landmine features using a forward-looking ground penetrating radar with MIMO array," *IEEE Trans. on Geosci. Remote Sens.*, Vol. 50, No. 10, 4135–4144, 2012.
21. Chen, B., T. Jin, Z. Zhou, and B. Lu, "Estimation of pose angle for trihedral in ultrawideband virtual aperture radar," *Progress In Electromagnetics Research*, Vol. 138, 307–325, 2013.
22. McCorkle, J. W., "Focusing of synthetic aperture ultra wideband data," *IEEE International Conference of Systems Engineering*, 1–5, 1991.
23. Yoon, Y. S. and M. G. Amin, "Behind-the-wall target indication (BWTI)," *Proc. SPIE Radar Sens. Technol. XIII Conf.*, 73080S1–73080S12, 2009.
24. Lu, B., Y. Zhao, X. Sun, and Z. Zhou, "Design and analysis of ultra wide band split transmit virtual aperture array for through the wall imaging," *International Journal of Antennas and Propagation*, 2013, Doi: 10.1155/2013/934509.
25. Wang, H., B. Lu, Z. Zhou, and Q. Song, "Through-the-wall imaging and correction based on the estimation of wall parameters," *Proceedings of 2011 IEEE CIE International Conference on Radar*, 1327–1330, 2011.
26. Dehmollaian, M. and K. Sarabandi, "Refocusing through building walls using synthetic aperture radar," *IEEE Trans. on Geosci. Remote Sens.*, Vol. 46, No. 6, 1589–1599, 2008.

27. Kong, J. A., *Electromagnetic Wave Theory*, EMW Publishing, Cambridge, MA, 2000.
28. Sun, X., B. Lu, T. Jin, and Z. Zhou, "A fast echo construction method in through the wall simulation and analysis," *Proceedings of Image Analysis Signal Processing*, 208–212, 2012.
29. Keller, J. B., "Geometrical theory of diffraction," *Journal of the Optical Society of America*, 116–130, 1962.
30. Jackson, J. A., B. D. Rigling, and R. L. Moses, "Canonical scattering feature models for 3D and bistatic SAR," *IEEE Transactions on Aerospace and Electronic Systems*, Vol. 46, No. 2, 525–541, 2010.
31. Taflove, A. and S. C. Hagness, *Computational Electrodynamics: The Finite-difference Time-domain*, Artech House, Boston, MA, 2000.
32. Dogaru, T. and C. Le, "SAR images of rooms and buildings based on FDTD computer models," *IEEE Trans. on Geosci. Remote Sens.*, Vol. 47, No. 5, 1388–1401, 2009.
33. Pena, D., R. Feick, H. Hristov, and W. Grote, "Measurement and modeling of propagation losses in brick and concrete walls for the 900-MHz band," *IEEE Trans. on Antennas and Propag.*, Vol. 51, No. 1, 31–39, 2003.